Exploring intense attosecond pulses

Exploring intense attosecond pulses

D Charalambidis[1,2,5]**, P Tzallas**[1]**, E P Benis**[1]**, E Skantzakis**[1,2]**,
G Maravelias**[1]**, L A A Nikolopoulos**[3]**, A Peralta Conde**[1]
and G D Tsakiris[4]

[1] Foundation for Research and Technology—Hellas, Institute of Electronic
Structure and Laser, PO Box 1385, GR-71110 Heraklion, Crete, Greece
[2] Department of Physics, University of Crete, PO Box 2208,
GR71003 Heraklion, Crete, Greece
[3] Department of Applied Mathematics and Theoretical Physics,
The Queen's University of Belfast, Belfast BT7 1NN, UK
[4] Max-Planck-Institut für Quantenoptik, D-85748 Garching, Germany
E-mail: chara@iesl.forth.gr

Abstract. After introducing the importance of non-linear processes in
the extreme-ultra-violet (XUV) spectral regime to the attosecond (asec)
pulse metrology and time domain applications, we present two successfully
implemented techniques with excellent prospects in generating intense asec
pulse trains and isolated asec pulses, respectively. For the generation of
pulse trains two-color harmonic generation is exploited. The interferometric
polarization gating technique appropriate for the generation of intense isolated
asec pulses is discussed and compared to other relevant approaches.

[5] Author to whom any correspondence should be addressed.

IOP Institute of Physics Φ DEUTSCHE PHYSIKALISCHE GESELLSCHAFT

Contents

1. Introduction

High brilliance extreme-ultra-violet (XUV)/x-ray radiation sources, such as synchrotron installations, have for many years largely served a number of scientific areas such as physics, chemistry, material sciences, biology and medicine. Investigations conducted with such sources were mainly focused on the structural properties of matter. Recent substantial progress in radiation source engineering led to the development of coherent XUV/x-ray sources of ultra-short pulse duration. Thus, a new dimension has opened up, namely that of the real time studies of ultra fast processes in this spectral region. The combined access to both structure and dynamics that these sources provide offers the possibility for complete four-dimensional studies in light–matter interactions at unprecedented resolution levels. While the new large-scale research infrastructures of free electron laser (XFELs) [1, 2] offer extreme brilliances at short wavelengths, tabletop laser-based XUV sources utilizing non-linear laser frequency up-conversion processes, such as higher order harmonic generation (HOHG) in gases [3, 4], known as gas harmonics, or on surface plasma [5]–[10] targets, provide unique attosecond (asec) scale temporal resolution. With their record of 130 as long XUV pulses [11], harmonics provide presently at least two orders of magnitude higher temporal resolution than XFELs. Although not yet fully proliferated, these tabletop sources reach today sub-μm^3/sub-fs spatiotemporal resolution and have the potential to improve it to the sub-Å^3/asec level.

Despite the outstanding potential of surface plasma harmonic emission towards intense asec pulse generation, so far asec pulses have been experimentally demonstrated only in harmonic emission from gases interacting either with few-cycle carrier-envelope-phase (CEP) stabilized pulses [12] or many-cycle pulses of high peak power laser systems [13]–[17]. While few-cycle pulses led to the generation of isolated asec pulses [18, 19] and produced a number of impressive proof of principle applications [20], their pulse energy is currently so low (at the pJ level) that all successful experiments had to be conducted in combination with the driving IR field. In contrast, harmonics produced by many-cycle high peak power laser pulses led so far to the generation of asec pulse trains, but at much higher pulse energies of the order of 1 μJ. The accessible focused XUV intensities may reach 10^{14} W cm^{-2} [21] and thus are by far sufficient in inducing non-linear XUV processes. Indeed, a number of multi-XUV-photon processes have been demonstrated utilizing single harmonics [22]–[25] or superpositions of harmonics [26]–[28]. These processes have been proven central to asec pulse metrology [29] and have paved the way to XUV-pump–XUV-probe applications. However, pulse trains reduce a lot the versatility of pump–probe experiments, whereas the development of energetic isolated XUV pulses would boost the investigation of few fs or sub-fs dynamics. The recently achieved

generation of coherent continua from many-cycle, high peak power laser pulses [30] is a decisive step towards this goal.

Asec research at FORTH-IESL is focused on the generation and applications of energetic vacuum-ultra-violet (VUV) and/or XUV asec and/or few fs pulses. Here, the term energetic implies that observable non-linear processes may be induced solely by the VUV/XUV radiation. This work discusses specific issues of our recent accomplishments on the investigation of such non-linear processes induced by asec pulse trains, and further presents new approaches that (i) lead to increased efficiencies in the generation of asec trains and (ii) enable the generation of energetic isolated asec pulses utilizing efficient polarization gating of many-cycle high peak power laser pulses. The generation of broadband continua using this approach is demonstrated while the potentiality of the method is discussed and compared to other implemented approaches.

2. Non-linear XUV processes

The indubitable observation of non-linear XUV processes is pivotal to asec pulse metrology and applications. In this section, we summarize successful experimental efforts in demonstrating two-XUV-photon processes induced by superposition of harmonics and their exploitation in asec science.

Non-linear interaction of XUV radiation with matter leads to ionization due to the large photon energy. In this spectral region, the interaction strength is such that ionization proceeds through multiphoton absorption unless the field intensity exceeds $10^{16}\,\mathrm{W\,cm^{-2}}$, a value not available yet in XUV laboratories. Moreover, the pulse duration is short enough for the ionization process to be governed by the peak intensity. The multiphoton ionization rate, well below its saturation limit, is given by:

$$\dot{N} = N\sigma^{(n)}F^n(t),$$

where N is the number of atoms in the interaction volume V, F the photon flux and $\sigma^{(n)}$ the generalized n-photon cross-section. For a second-order process $\sigma^{(2)}$ has small values ranging from 10^{-49} to $10^{-52}\,\mathrm{cm^4\,s}$ for a range of excess energies from zero to the ionization energy ([31] and references therein). Thus, for a realistic atomic density n_a (e.g. 10^{15}–$10^{16}\,\mathrm{atoms\,cm^{-3}}$) and interaction volume, a non-saturated observable two-photon ionization yield

$$N_{\mathrm{ION}} = n_a V \sigma^{(2)} \int_{-\infty}^{\infty} F^2(t)\mathrm{d}t$$

requires high XUV intensities, well exceeding $10^8\,\mathrm{W\,cm^{-2}}$. This is the reason why the observation of two-XUV-photon processes has been a formidable target of intense experimental efforts for about two decades.

The first demonstration of a two-XUV-photon ionization (TXUVPI) of an atom by an asec pulse train was achieved in 2003 [26]. Helium atoms were ionized by a superposition of the 7th to the 13th harmonic of the 0.375 PHz driving laser field frequency, in a non-resonant one harmonic photon absorption below the ionization threshold, followed subsequently by the absorption of a second photon of any of the harmonics available. The key parameter in this and all other experiments that followed has been the loose focusing conditions in the harmonic generation region. The thus increased interaction volume led to the XUV photon numbers

and intensities required for the observation of a non-linear XUV process. Loose focusing is possible when excess energy is available in the laser pulses so that intensities just below the ionization saturation intensity can be reached by long focal lengths. In this first experiment, the total He ion yield was measured as a function of the ionizing intensity. It has been recently repeated in an energy resolved manner [28]. While the observation of the two-XUV-photon total ionization yield has established the platform for the temporal characterization of asec pulse trains via the second-order autocorrelation (AC) technique [14, 17], the energy resolved spectra was a step towards a second-order FROG-like [32] measurement (FROG stands for frequency resolved optical gating) in the XUV spectral region. The photoelectron energy resolution in the experiment of [28] was not sufficient for a FROG measurement, i.e. the photoelectron peaks were broader than the width of each individual harmonic. Nevertheless, for an isolated asec pulse, i.e. for a broadband continuum, even a low-energy resolution of the photoelectron spectrometer is ample for a FROG measurement and thus for a detailed temporal reconstruction of asec waveforms.

The realization of the TXUVPI of He was one of the central prerequisites for the breakthrough of the second-order AC of an asec pulse train. In the following, we will discuss the results of this experiment from a different point of view, namely that of the observation of the dynamics of an electromagnetically driven electronic wavepacket. In other words, the approach used for the measurement of the duration of the asec bursts simultaneously serves for the investigation of ultra-fast electron dynamics and thus can be viewed as an application of asec pulses. This is because the temporal characteristics of the pulse are imprinted on the evolution of the electronic wavepacket.

In the second-order AC experiment in He, absorption of the first photon from the harmonic superposition is non-resonant. Thus, a virtual state is excited, which is the superposition of all allowed atomic states. In the presence of the field of the harmonics, excitation amplitudes and populations will obey Rabi oscillations. Since excitation is non-resonant, the corresponding Rabi frequencies, for the XUV intensities available, will be equal to the detuning of each harmonic from the allowed real states, 1s2p being the closest one and thus the one with the highest amplitude. The excitation dynamics will thus be determined by a linear combination of Rabi oscillations with frequencies that differ by twice the laser frequency. This leads to a temporal beating of the excitation amplitudes similar to that of the beating of the fields of the harmonic superposition. A fast driven electronic wavepacket is excited, the temporal evolution of which follows the envelope of the beating of the harmonic superposition field. In fact, taking into account both co- and counter-rotating terms, it turns out that the electronic wavepacket undergoes a small amplitude fast oscillation as well, corresponding to the fast oscillation of the field carrier. This is shown in figure 1, in which the blue line is the square of the driving field and the green line depicts the population of the 1s2p state calculated by solving the time-dependent Schrödinger equation (TDSE) within the electric dipole approximation of the interaction of He with the superposition of the harmonics. The set of the harmonic amplitudes are those reported in [14], while the corresponding phases are set equal. As can be seen, the 1s2p population to a large extent follows the intensity oscillations. While the intensity envelope and the population modulation are almost identical, a signature of the fast oscillations of the carrier can also be found in the 1s2p population, which however does not fully return to the ground state in each cycle. In other words, the excited electron wavepacket has a temporal evolution that follows the envelope and thus the asec beating of the driving field, with some additional small amplitude ripples at the carrier frequency.
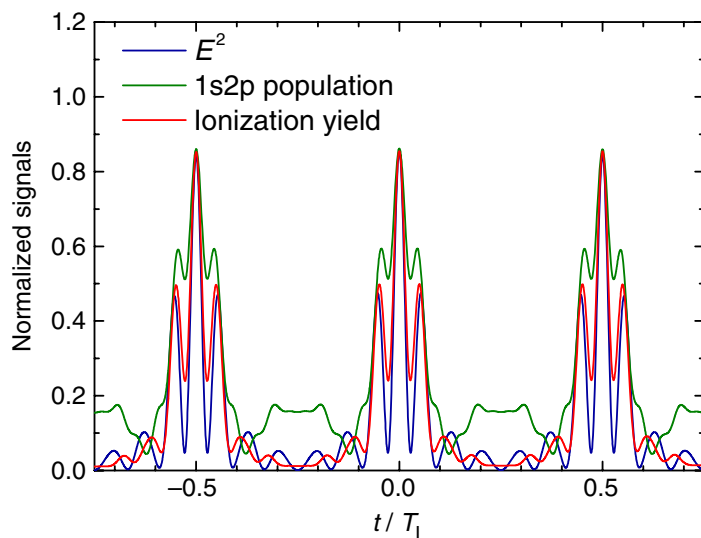
Figure 1. Comparison of the temporal evolution of the 1s2p population (green line), the ionization yield (red line) and the instantaneous ionizing field intensity (square of the E-field) (blue line). The population of the excited state follows the envelope of the square of the E-field and to some extent the instantaneous ionizing field intensity without however reaching zero in each half cycle. The ionization yield is closer to the oscillatory behavior of the square of the field. T_L is the laser period.

The second delayed XUV pulse of the autocorrelator excites a replica of the wavepacket phase shifted according to the introduced delay between the two excitation pulses. The interference of the two wavepackets is probed through its ionization in the second step of the two-photon absorption process as a function of the delay. This is equivalent to the ionization yield evolution shown in figure 1 by the red line that practically behaves like the field intensity. In other words, the second-order AC experiment can be interpreted as a 'Ramsey' type experiment in which fringing reflects the dynamics of the driven bound electron wavepacket excited by single photon absorption of the harmonic superposition. In this context, the second-order AC measurement is simultaneously an application of an asec pulse train in observing the ultrafast dynamics of a driven electron wavepacket in an atom. It is worth noting that if the excitation process is near resonant or resonant the envelope of the Ramsey fringes also contains information about the temporal characteristics of the intermediate state, which in some cases can be deconvoluted from the trace. Furthermore, for pulse durations much smaller than the evolution time of the intermediate state it turns out that both the pulse duration and the characteristic time of the state can be deduced from the same measured AC trace. In this framework, we are currently working on a further application towards the determination of ultra-short molecular dissociation times applying the same approach in a two-VUV-photon molecular ionization scheme, in which absorption of the first photon is resonant with the dissociative state [33].

However, the He experiment described above is a special case for which a pulse train can be used. In general, it is much more convenient to accomplish a time domain measurement using

isolated asec pulses of sufficient intensity. A route for the synthesis of such pulses is described in section 4 of this work.

One of the questions raised immediately after the implementation of the second-order AC was on the general applicability of the method. Two-photon ionization sets a limit to the photon energy range that can be characterized. The method is applicable as long as the highest photon energy contained in the asec pulse is smaller than the ionization energy of the medium. Helium has the highest ionization threshold and that is why it has been chosen as the target medium. However, the method may be extended to shorter wavelengths, exploiting other non-linear processes such as multiple direct ionization, taking advantage of the higher values of the multiple ionization thresholds. The available harmonic intensities are sufficient to induce this type of non-linear process as well. In this context, we have recently demonstrated direct double ionization of Kr and Ar by a superposition of gas harmonics [27]. Direct multiple (triple and so on) ionization would further extend the photon energy range that can be characterized, provided that sufficient XUV intensities are available. An alternative process is two-photon ATI [34]. Utilizing this type of process, second-order AC-based techniques will be applicable to the entire XUV/x-ray spectral regime.

3. Two-color enhanced HOHG towards intense asec pulse trains

The process of HOHG by the interaction of a two-color field with a gas phase medium brought two important issues into consideration for the asec community: the enhancement of the harmonic generation efficiency and the temporal structure of the emitted XUV radiation. The enhancement of the HOHG has been observed in several experiments both for parallel and perpendicularly linearly polarized two-color fields [35]–[40]. Theoretical studies have also predicted an enhancement of the harmonic generation by two orders of magnitude as compared to the single color field generation [35], [41]–[47]. In addition, generation of a strong asec pulse train has been predicted in the case of perpendicularly polarized two-color driving fields [40]. In this section, we experimentally investigate the enhancement of the harmonic generation by using two-color laser fields with parallel linear polarizations and study the dependence of the HOHG efficiency on the relative phase between the two superimposed fields. In a step further, we examine the temporal structure of the emitted XUV radiation in simulations based on the three-step model.

The experimental set-up used for tailoring a linearly polarized two-color field and its use for harmonic generation is shown in figure 2. Laser pulses of 50 fs duration, 800 nm wavelength and 300 μJ energy delivered by a 1 kHz Ti:sapphire laser system were used. A laser pulse is equally divided into the two arms of the two-color Michelson-type interferometer. In the first arm, the propagated fundamental pulse exits the interferometer after being transmitted through the harmonic separator (HS). In the second arm, the fundamental pulse is frequency-doubled in a type-I BBO crystal with ~30% conversion efficiency and exits the interferometer after being reflected at the HS. High reflectivity at 400 nm mirrors and HS are used in this arm in order to separate the second harmonic from the fundamental. The relative polarization of the two fields is set parallel by using a $\lambda/2$ plate in the interferometer arm of the fundamental pulse.

The outgoing pulse is focused by a 5 cm focal length Al coated spherical mirror into a gas cell filled with 100 mbar of Xe gas in which the harmonic generation occurs. The generated harmonic radiation is then monitored by an XUV monochromator. The intensity of the two
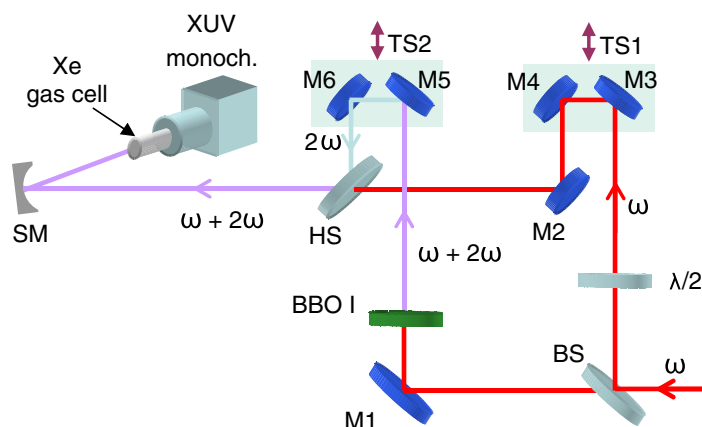
Figure 2. Two-color interferometer set-up. The fundamental- and second-harmonic frequencies are denoted by ω (red line) and 2ω (blue line), respectively. The purple line depicts the superposition of the two-color fields. BS: 50% beam splitter. M1, 2, 3, 4: flat mirrors for the reflection of the ω frequency. M5, 6: flat mirrors for the reflection of the 2ω frequency. TS1: piezoelectric translation stage. TS2: translation stage. HS: harmonic separator for the reflection of 2ω and the transmission of ω. SM: spherical metal mirror with 5 cm focal length. The angle between the incident and reflected two-color beam on the SM mirror was $\sim 4°$.

fields at the focus is $\sim 5 \times 10^{13}\,\mathrm{W\,cm^{-2}}$ for each color, a value which is close to the saturation intensity of Xe ionization. A $\sim 20\,\mu$m diameter pinhole is placed at the focus of the beam located at the exit of the gas cell in order to maximize the harmonic generation and to isolate the monochromator from the gas cell.

Figure 3(a) shows the recorded harmonic spectra generated by the two-color field (blue dashed line) and the fundamental laser pulse alone (black solid line). It is worth mentioning that both even and odd harmonics are produced by a two-color field as opposed to the single-color case due to field symmetry considerations.

In both spectra, the intensity ($1 \times 10^{14}\,\mathrm{W\,cm^{-2}}$) and the interaction volume in the harmonic generation region were approximately equal. In the case of the two-color field, the total harmonic signal is an order of magnitude larger as compared to that generated by the fundamental laser pulse. Figure 3(b) shows the same spectra as figure 3(a) multiplied by the spectral transmission function of a 200 nm thick In filter. Thus, the generated harmonics are restricted to be from 7th to 15th, a superposition that can be second-order autocorrelated towards a direct determination of its temporal characteristics [14, 17, 29].

The enhancement of the harmonic signal proved to be very sensitive to the relative phase ϕ between the two colors in the bichromatic field. Figure 3(c) depicts the harmonic spectra in the In filter transmission spectral region for two different values of the relative phase. Figures 4(a)–(d) show the dependence of the individual 8th, 9th, 10th and 11th harmonic signals on the relative phase ϕ, respectively. In all traces, ϕ has been arbitrarily set equal to zero at the minimum of the modulation of the signal. The modulation is found to be periodic with period of π and very sensitive to the spatiotemporal overlap of the two-color fields at the interaction region. Such behavior of the modulation of the individual harmonic signals in the
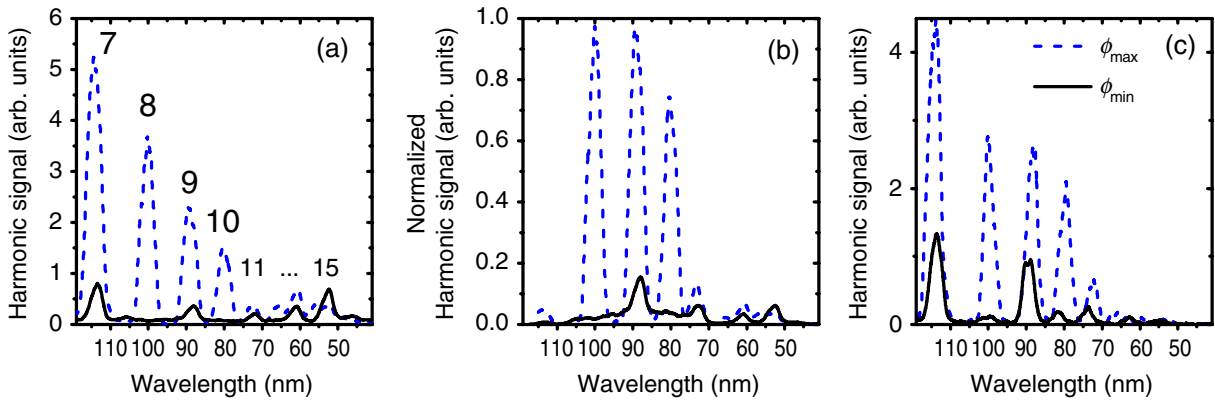
Figure 3. (a) Blue dashed line: harmonic spectrum recorded using the two-color field. Black solid line: harmonic spectrum recorded using only the fundamental pulse having the same intensity and interaction volume as the two-color field. (b) Harmonic spectra from the two-color field multiplied by the spectral transmission function of a 200 nm thick In filter. (c) Harmonic spectra for two different values of the relative phase ϕ between the two-color field. The blue dashed line corresponds to a ϕ value with maximum harmonic signal, while the black line corresponds to a value with minimum harmonic signal.
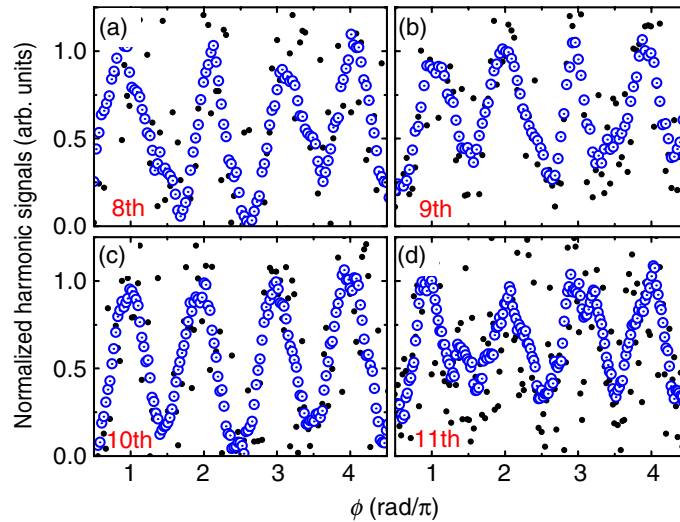

Figure 4. Dependence of the 8th to 11th harmonic signals on the relative phase ϕ between the two-color fields. The black dots correspond to the data points and the blue circles to an average of 10 data points. In all traces ϕ has been set equal to zero at the minimum of the signal modulation. A modulation of the signal with period π is observed.

plateau and cut-off spectral region has been observed and examined in detail earlier [39]. In the present experiment, using optimum spatiotemporal overlapping conditions, the modulation depth $M_q = 2 (S_{MAX} - S_{MIN})/(S_{MAX} + S_{MIN})$ has been measured to be $\sim$150% for the 8th and 10th harmonics while $\sim$90% for the 9th and 11th.

Actually, the periodicity of π observed in the XUV yield data is easily understood assuming a linear superposition of two fields with amplitudes E_{01} and E_{02} and frequencies ω and 2ω, respectively. The total field then reads

$$E(t) = E_{01}\cos(\omega t) + E_{02}\cos(2\omega t + \phi), \tag{1}$$

for which the periodic condition $E(\omega t + \pi, \phi) = -E(\omega t, \phi + \pi)$ is valid. This periodicity implies that the harmonic yield could be controlled by the phase difference between the two components of the pulse. However, this does not *a priori* account for the temporal structure of the XUV pulse composed by the produced harmonics.

In order to investigate the temporal structure of the formed XUV pulse the very successful, in single-color fields, three-step model is adopted. Thus, a two-color field described by equation (1) letting $E_0 = E_{01} = E_{02}$ in accordance with the experimental conditions is assumed. After solving the equation of motion $eE(t) = m\ddot{x}(t)$ for the above field for the tunneling conditions $\dot{x}(t_0) = 0 = x(t_0)$, where t_0 is the tunneling time, the displacement $x(t)$ is obtained as:

$$\frac{x(t)}{x_0} = \cos(\omega t_0) - \cos(\omega t) + \sin(\omega t_0)(\omega t_0 - \omega t)$$

$$+ \tfrac{1}{4}[\cos(2\omega t_0 + \phi) - \cos(2\omega t + \phi) + 2\sin(2\omega t_0 + \phi)(\omega t_0 - \omega t)], \tag{2}$$

where $x_0 = eE_0/m\omega^2$. The recombination time for an electron is determined after numerically solving equation (2) for $x(t) = 0$. Then the kinetic energy for the recombined electron (corrected for the ionization potential I_P) is calculated as

$$E_{\text{KIN}} = 2Up(\omega)\{\sin(\omega t) - \sin(\omega t_0) + \tfrac{1}{2}[\sin(2\omega t + \phi) - \sin(2\omega t_0 + \phi)]\}^2 + I_P,$$

where $Up(\omega) = e^2 E_0^2/4m\omega^2$ is the quiver energy for the fundamental field. Assuming a superimposed set of 9th to 15th harmonics with equal amplitudes and phases determined by the recombination time of the first revisit to the parent ion, the XUV pulse is reconstructed. Phase ϕ is reserved as the free parameter. The intensity of each color is set to $5 \times 10^{13}\,\text{W cm}^{-2}$, according to the experimental values.

Calculations have shown that formation of ultra-short pulses is possible in the two-color scheme. In figures 5(a) and (b) two indicative examples of clear formation and of essential absence of asec pulses, respectively, are shown. The temporal structure has been studied as a function of the relative phase ϕ and is shown in figure 5(c).

Notice that the periodicity of π seen in the graph originates from the intrinsic properties of the superimposed two-color field as for the harmonics yield modulation. The results of the three-step model show that the formation of ultra-short pulses is possible for a wide range of relative phases. Even though this semi-classical model is simplistic and does not account for propagation effects, it is indicative of the potentiality in forming asec pulses by two-color fields and worth further attention both theoretically and experimentally.

4. A new route towards intense isolated asec pulses

All asec non-linear XUV processes demonstrated so far are induced by pulse trains. However, for applications based on non-linear processes, in particular for pump–probe experiments, pulse trains are inconvenient. Such experiments would substantially benefit from the development of
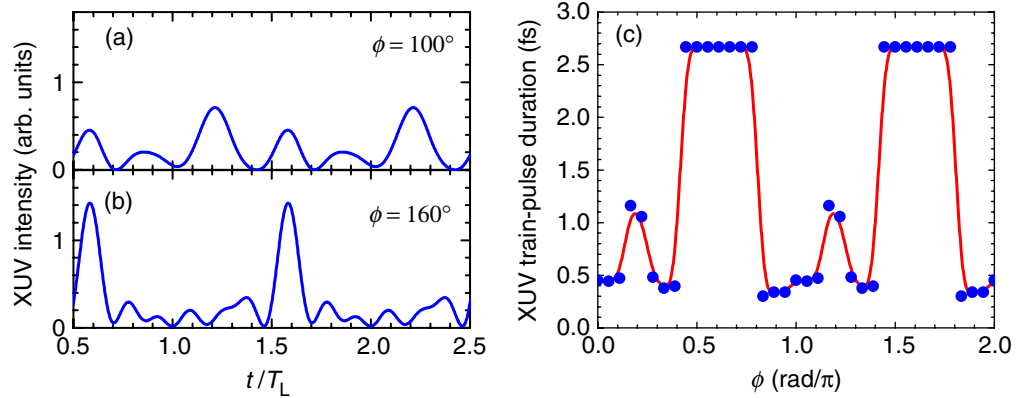
Figure 5. (a, b) Calculated harmonic pulses formed by a two-color field. They are superimposed by the 9th to 15th harmonics of equal amplitudes and phases determined by the three-step model (see text for details). Two indicative examples of structured and non-structured pulses determined by the phase difference ϕ between the two color fields are shown. (c) Estimation of the pulse duration as a function of ϕ. Data points at the duration value of the fundamental laser period 2.667 fs represent pulses showing insignificant temporal structure.

intense isolated asec pulses. Towards this goal, two different approaches are currently under consideration for gas harmonics. Either by developing high peak power few-cycle fsec laser systems or by restricting the emission time to an ultra-short time fraction of a high power many-cycle laser systems. The latter can be achieved by a technique initially proposed by Corkum *et al* [48], which is established under the term 'polarization gating'. This technique exploits the strong dependence of the harmonic generation on the ellipticity (ε) of the driving laser field. A fast varying ellipticity can thus act as a shutter in the XUV generation process. By forming an ellipticity modulated driving laser pulse, depicting linear polarization only at its central part, a few fs long time gate τ_g can be created during which the shutter is open. In this way, the XUV emission may be temporally confined to half a laser cycle, having a broadband continuum spectrum and a temporal envelope of a single asec pulse.

Polarization gating has been successfully implemented in producing broadband continuum XUV radiation [30, 49], as well as the shortest ever XUV pulse [11], using 5 fs long CEP stabilized laser pulses and a very convenient experimental set-up simply based on two waveplates. Two delayed and partially overlapping pulses with perpendicular polarization produced by the first birefringent plate synthesize a pulse with variable ellipticity ε that reaches unity at the center. The second waveplate ($\lambda/4$) reverses the ellipticity to linear at the center and circular/elliptical elsewhere. However, this method is essentially applicable only to few-cycle driving pulses. This is because the gate width produced by the method [49] reads

$$\tau_g \cong \frac{0.15\tau^2}{\Delta t \ln 2},$$

where τ is the initial pulse width and Δt the delay between the two pulses. This relation implies that in order to maintain the gate width narrow while increasing the pulse width, the delay Δt has to be increased to very large values, leading to an overlap of only the very far pulse
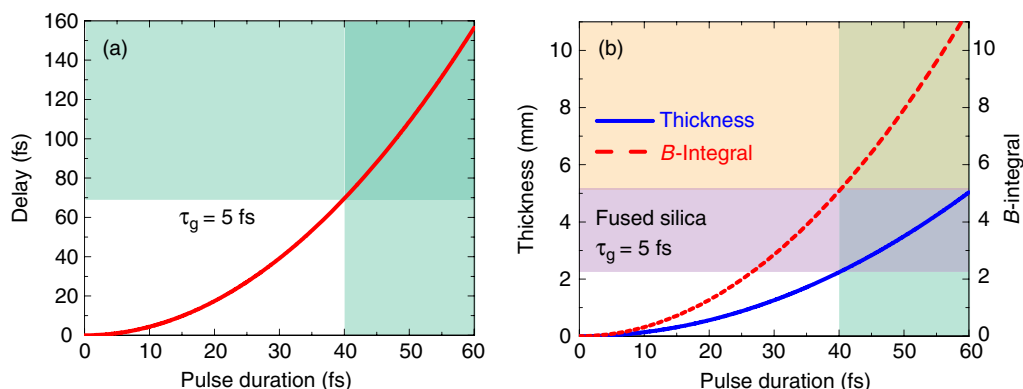
Figure 6. (a) Delay between the two pulses in the wave-plate polarization gating approach required for a gate width of 5 fs as a function of the pulse width. For widths between 40 and 60 fs this delay is about twice the pulse width. (b) Plate thickness (blue solid line) and corresponding B-integral (red dashed line) for an intensity of $1\,\mathrm{TW\,cm^{-2}}$ in the wave-plate polarization gating approach required for a gate width of 5 fs as a function of the pulse width. For widths between 40 and 60 fs the B-integral values range from about 5 to 11, i.e. above the tolerance threshold.

edges and thus to a very low conversion efficiency. The relation between Δt and τ for a gate width $\tau_g = 5\,\mathrm{fs}$ is depicted in figure 6(a). For typical 40–60 fs pulse widths of high peak power laser systems, the required delay ranges between 70 and 160 fs imposing in practice no overlap between the two pulses.

The restriction of the method to few-cycle pulses, which at present have limited energy content (less than 1 mJ at 5 fs, with the exception of the 7.6 fs 15.5 mJ system of the Vrije Universitat [50]), is prohibitive for energetic asec pulse generation. An additional drawback of the waveplate approach when applied to many-cycle high peak power pulses is that it inevitably leads to large B-integral values exceeding by far the safety threshold. The situation is illustrated in figure 6(b). For 40–60 fs long pulses, the first fused silica waveplate thickness has to be between 2 and 5 mm in order to achieve a 5 fs gate. For an intensity of $1\,\mathrm{TW\,cm^{-2}}$ the B-integral corresponding to this thickness ranges between 5 and 11, much larger than the allowed threshold.

We have recently developed an alternative interferometric polarization gating (IPG) approach, the gate of which is substantially less sensitive to the pulse duration. The method is thus applicable to many-cycle pulses as well, the peak power of which may reach hundreds of TW. The essence of the method is the synthesis of an ellipticity modulated pulse from four individually controlled linearly polarized pulses of variable field amplitude, relative polarization and delay. The method is schematically shown in figure 7.

The four pulses originate from the same initial laser pulse. Two of them are co-propagating and delayed with respect to each other by an odd number of half laser periods, so that their overlapping parts form a destructive interference minimum. This minimum will play the role of a mould for the gate. Its steepness can be controlled by the variable delay and becomes maximum when the delay is of the order of the initial pulse width. The delay between the other two pulses is of the same order of magnitude but such that their interference is constructive.
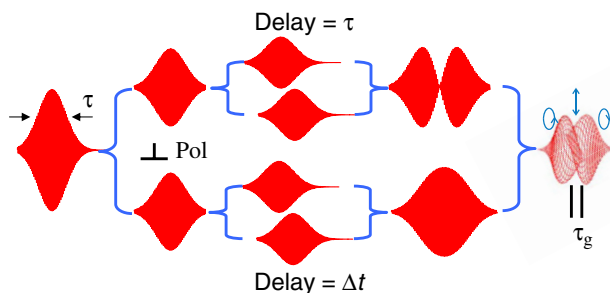
Delay = τ

$\perp$ Pol

Delay = Δt

Figure 7. Schematic representation of the interferometric polarization technique. One pulse is split into four. Two of the appropriately delayed pulses interfere constructively, while the other two form a destructive interference minimum. The polarization planes of the superpositions are mutually perpendicular. The two waveforms are superimposed forming an ellipticity modulated pulse with linear polarization in its central part.
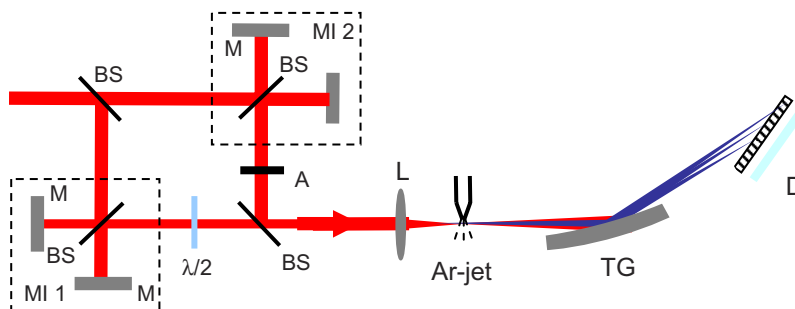
Figure 8. Experimental set-up. The two-Michelson IPG set-up (BS: beam splitter, M: mirrors, A: attenuator, MI: Michelson interferometer), and the harmonic generation and observation set-up (L: lens, TG: toroidal grating, D: multi-channel plate detector with phosphor screen).

The polarization planes of the two resulting superposition fields are subsequently rotated so as to become perpendicular. Obviously, when these two fields are recombined with zero delay with respect to each other (or with a delay equal to an integer number of laser periods) they synthesize an ellipticity modulated pulse, depicting linear polarization only in its central part.

The detailed width and power content of the gate depends on the relative delay and amplitudes of the superimposed pulses. This dependence has been published elsewhere [30]. A reduction of the gate width comes at the cost of the power content of the gate.

IPG has been implemented utilizing two Michelson interferometers described elsewhere [30]. With this set-up efficient polarization gating has been demonstrated through the transition from a discrete harmonic spectrum (harmonics 15th to 23rd) to a broadband XUV continuum [30] spanning over ~15 eV. An illustration of the two-Michelson arrangement, the generation and the detection units is shown in figure 8. The ratio of the power within the 5 fs long output gate to the total incoming power was about 0.035.

The XUV radiation is produced in a pulsed Ar gas jet using a 10 Hz repetition rate Ti : sapphire laser system delivering 50 fs long pulses of up to 150 mJ energy. The spectra

are recorded with a home made grazing incidence XUV monochromator equipped with a Jobin Ivon toroidal grating, using a position sensitive detector (MCP assembly with a phosphor screen anode read out by a CCD camera) placed tangentially to the Roland circle of the grating. No absolute XUV photon number measurement has been performed in this experiment.

An interesting aspect of the results obtained is that when recording is shot to shot the CEP variation is imprinted in the spectra. They vary from continuum to semi-discrete, while the semi-discrete spectra depict shot to shot variable peak positions [30]. This behavior is due to the shot to shot variation of the relative CEP of the laser. Observed CEP effects in the multi-optical-cycle regime are rare [51]. Thus the general belief is that CEP plays no role when using many-cycle pulses. The present result together with the work of Sansone *et al* [51] invalidate this assumption. The reason is that the narrow gate introduced makes the conditions equivalent to those when using few-cycle pulses. Indeed, the destructive interference minimum along with the gate phase is locked to the envelope phase (the minimum is equidistant from the positions of the peak maxima of the two interfering pulses), while the constructive interference maximum and thus the quasi-linearly polarized driving field phase is locked to the carrier phase. The variation of the single shot harmonic spectra due to the CEP variation may serve as a rough measure of the gate width. It is worth noting that if the maximum possible gate power content is not required, by narrowing the gate width the emission may become digital, i.e. either emission of an XUV continuum or essentially no XUV emission. The emitted continuum is coherent and thus forms an ultra short isolated pulse the duration of which remains to be measured. The method will highly benefit from a future CEP stabilization of high peak power laser systems. Until then, pulse metrology and pump–probe applications will have to rely on discrimination approaches, e.g. utilizing the XUV spectra as a monitor of the CEP and their discrete or continuum character as the discriminator condition.

An additional advantage of the method is that it may be implemented through set-ups avoiding 'thick' optical elements. Pellicles may be used as beam splitters or thin plates as retarders keeping the *B*-integral to acceptable values.

The disadvantages associated with IPG are the current absence of CEP stabilized high peak power laser systems and the long-term stability of the experimental set-up. The latter may be substantially improved by the alternative set-up shown in figure 9. It is a Mach–Zehnder arrangement that takes advantage of the fact that whenever constructive interference occurs at the exit arm of a collinear interferometric set-up destructive interference occurs at the second arm. In principle, there is no need to use two interferometers in order to form the two fields. They are both available at the two exits of one and the same interferometer.

In a Michelson interferometer, the radiation in the second exit arm counter-propagates the incoming beam, thus becoming less convenient for use. In the Mach–Zehnder arrangement shown, the pulses of both exit arms can be exploited. Indeed, when the first pulse after the beam splitter BS_2 depicts a destructive interference minimum the second one will have a constructive interference maximum. These two pulses are formed through recombination at the beam splitter BS_2 of pulses appropriately delayed in the Mach–Zehnder interferometer. Variable delay is here introduced by BK7 plates of through rotation variable thickness. The I_1/I_2 ratio can be adjusted by the last beam splitter (BS_3). The appropriate value of this ratio depends on the initial pulse duration. The 20–80% ratio given in figure 9 is for the 50 fs initial pulse duration. The set-up presented is simpler, more stable and has a factor of two higher throughput than the double Michelson arrangement. The only disadvantage of this set-up is that the delay of all four pulses
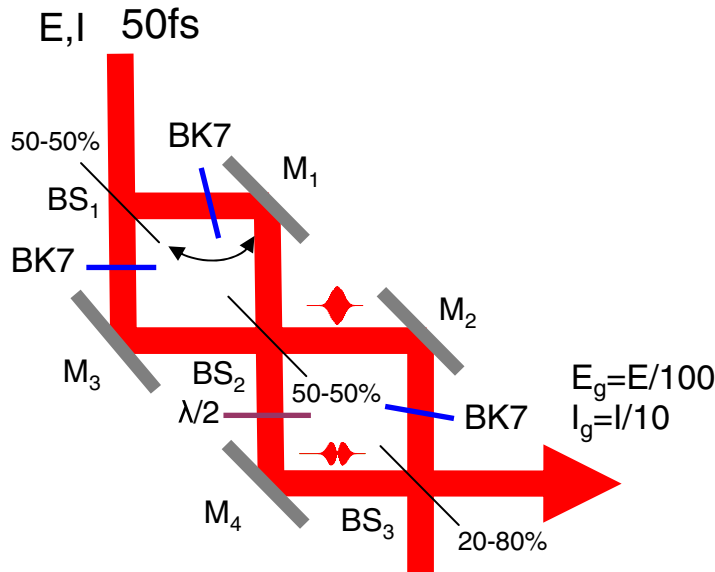
Figure 9. IPG set-up. The pulse is split into two by the beam splitter BS_1 of the Mach–Zehnder interferometer. The two pulses, appropriately delayed, recombine at the beam splitter BS_2. The two pulses of the two branches after BS_2 depict a constructive and a destructive interference minimum at their central part respectively. The $\lambda/2$ plate rotates the polarization plane in one of the branches. The two wave forms recombine at the beam splitter BS_3. The output pulse has the required ellipticity modulation. For a 50 fs input pulse, the energy content of a 5 fs gate is about two orders of magnitude smaller than the input energy and the gate intensity about one order of magnitude lower than the input intensity.

cannot be separately adjusted. The two pulses synthesizing the first field and those synthesizing the second field have the same (variable) delay. However, this is not a critical factor. Such a set-up is currently under construction and will be used towards non-linear XUV experiments with isolated asec pulses.

A comparison between the different polarization gating approaches is summarized in figure 10. The gate intensity content I_g/I_{in}, where I_g is the intensity of the driving laser field within τ_g and I_{in} is the total incoming intensity, respectively, drops fast with pulse duration in the waveplate method, while for both IPG set-ups the reduction is rather slow. Above 30 fs both IGP methods have a higher I_g/I_{in} ratio than the waveplate approach, while the Mach–Zehnder set-up remains superior for any pulse duration. Given the fact that currently I_{in} is much higher in high peak power many-cycle than in few-cycle pulses, both IPG approaches secure much higher I_g values and thus more intense asec pulses. To give an example from a 20 TW system (e.g. 1 J, 40 fs), one may reach gate power content $\sim$2 TW (10 mJ, 5 fs) with low B-integral value arrangements. A necessary prerequisite for that is that the target medium is not depleted. For atomic targets ionization from the elliptically polarized part of the pulse may deplete the target. This problem may be avoided by reducing the intensity while keeping the power high. This is always possible by using looser focusing and enlarged target areas. Finally, the target
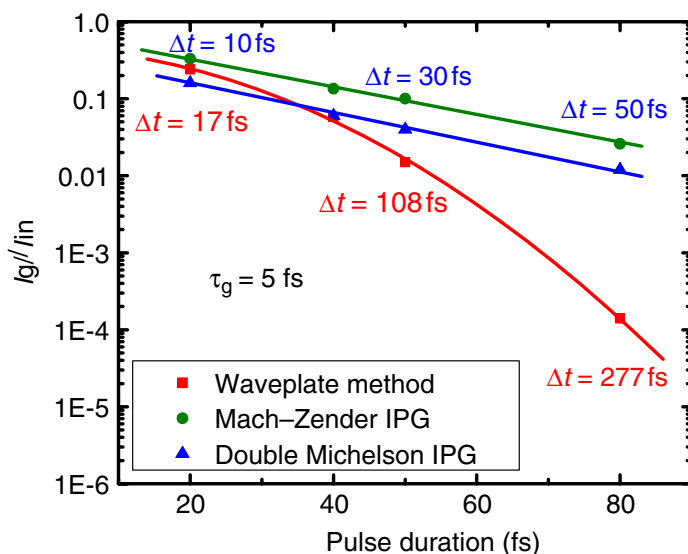
Figure 10. Comparison of the ratio of the gate intensity content I_g/I_{in} to the input intensity of the different polarization gating set-ups as a function of the pulse duration.

depletion problem is eliminated when using solid targets as in the generation of harmonics from surface plasma for which the IPG method is highly beneficial [52].

5. Conclusions

We have discussed recent accomplishments in non-linear XUV processes in the context of their importance to asec pulse metrology and time domain applications, and of the parameters required for versatile use of them. We so far achieved XUV intensity levels of asec pulse trains close to $10^{13}\,\text{W cm}^{-2}$, with which a number of two-XUV-photon processes induced by harmonic superpositions have been demonstrated. An increase of this intensity would obviously be beneficial for applications, but what is more important is the generation of isolated asec pulses that when focused may reach intensities of this or higher level. We have presented and discussed approaches serving both goals. The results of two-color (ω, 2ω) harmonic generation indicate that, when combined with loose focusing geometries exploiting high peak power, the XUV focused intensities may exceed $10^{14}\,\text{W cm}^{-2}$. As for the generation of isolated asec pulses, the IPG technique turns out to be particularly promising, as it avoids important limiting factors of other existing polarization gating approaches when they are applied to many-cycle high peak power pulses. Further to gas harmonics it is highly adequate for harmonics emitted from surface plasma and asec pulse generation. It is worth noting here that this technique can be used in many existing high peak power systems by simply adding a small-scale optical set-up at their exit, thus leading to gates of 5 fs at the TW level. The lack of stabilized CEP in such systems is a drawback and its stabilization is a forthcoming challenge.

IOP Institute of Physics ⬤ DEUTSCHE PHYSIKALISCHE GESELLSCHAFT

Acknowledgments

References

[1] Pantell R H, Soncini Y and Putoff H E 1968 *IEEE J. Quantum Electron.* **4** 905
[2] Deacon D A G *et al* 1977 *Phys. Rev. Lett.* **38** 892
[3] McPherson A *et al* 1987 *J. Opt. Soc. Am.* B **4** 595
[4] Ferray M *et al* 1988 *J. Phys. B: At. Mol. Opt. Phys.* **21** L31–5
[5] Bulanov S V, Naumova N M and Pegoraro F 1994 *Phys. Plasmas* **1** 745
[6] Lichters R *et al* 1996 *Phys. Plasmas* **3** 3425
[7] Tsakiris G D *et al* 2006 *New J. Phys.* **8** 19
[8] Dromey B *et al* 2006 *Nat. Phys.* **2** 456
[9] Quere F *et al* 2006 *Phys. Rev. Lett.* **96** 125004
[10] Thaury C *et al* 2007 *Nat. Phys.* **3** 424
[11] Sansone *et al* 2006 *Science* **314** 443
[12] Baltuska A *et al* 2003 *Nature* **421** 611
[13] Papadogiannis N A *et al* 1999 *Phys. Rev. Lett.* **83** 4289
[14] Tzallas P *et al* 2003 *Nature* **426** 267
[15] Paul P M *et al* 2001 *Science* **292** 1689
[16] Mairesse Y *et al* 2003 *Science* **302** 1540
[17] Nabekawa Y *et al* 2006 *Phys. Rev. Lett.* **96** 083901
[18] Hentschel M *et al* 2001 *Nature* **414** 509
[19] Kienberger R *et al* 2002 *Science* **297** 1144
[20] Uiberacker M *et al* 2007 *Nature* **446** 627
[21] Mashiko H *et al* 2004 *Opt. Lett.* **29** 1927
[22] Xenakis D *et al* 1996 *J. Phys. B: At. Mol. Opt. Phys.* **29** L457
[23] Kobayashi Y *et al* 1998 *Opt. Lett.* **23** 64
[24] Miyamoto N *et al* 2004 *Phys. Rev. Lett.* **93** 083903
[25] Nabekawa Y *et al* 2005 *Phys. Rev. Lett.* **94** 043001
[26] Papadogiannis N A *et al* 2003 *Phys. Rev. Lett.* **90** 133902
[27] Benis E P *et al* 2006 *Phys. Rev.* A **74** 051402
[28] Benis E P *et al* 2006 *New J. Phys.* **8** 92
[29] Nikolopoulos L A A *et al* 2005 *Phys. Rev. Lett.* **94** 113905
[30] Tzallas P *et al* 2007 *Nat. Phys.* **3** 846
[31] Papadogianis N A *et al* 2003 *Appl. Phys.* B **76** 721
[32] Trebino R *et al* 1997 *Rev. Sci. Instrum.* **68** 3277
[33] (to be published)
[34] Hasegawa H *et al* 2005 *Phys. Rev.* A **71** 023407
[35] Eichmann H *et al* 1995 *Phys. Rev.* A **51** R3414
[36] Kondo K *et al* 1996 *J. Opt. Soc. Am.* B **13** 424
[37] Perry M D and Crane J K 1993 *Phys. Rev.* A **48** R4051
[38] Watanabe S *et al* 1994 *Phys. Rev. Lett.* **73** 2692
[39] Andiel U *et al* 1999 *Europhys. Lett.* **47** 42
[40] Kim I J *et al* 2005 *Phys. Rev. Lett.* **94** 243901

IOP Institute of Physics ⏀ DEUTSCHE PHYSIKALISCHE GESELLSCHAFT

[41] Paulus G G, Becker W and Walther H 1995 *Phys. Rev.* A **52** 4043
[42] Protopapas M *et al* 1995 *Phys. Rev.* A **52** R2527
[43] Telnov D A, Wang J and Chu S J 1995 *Phys. Rev.* A **52** 3988
[44] Cormier E and Lewenstein M 2000 *Eur. Phys. J.* D **12** 227
[45] Figueira de Morisson Faria C *et al* 1999 *Phys. Rev.* A **55** 1377
[46] Figueira de Morisson Faria C *et al* 2000 *Phys. Rev.* A **61** 063415
[47] Kim C M, Kim I J and Nam C H 2005 *Phys. Rev.* A **72** 033817
[48] Corkum P B, Burnett N H and Ivanov M Y 1994 *Opt. Lett.* **19** 1870
[49] Sola I J *et al* 2006 *Nat. Phys.* **2** 319
[50] Witte S *et al* 2007 *Opt. Express* **14** 8168
[51] Sansone G *et al* 2004 *Phys. Rev. Lett.* **92** 113904
[52] Baeva T *et al* 2006 *Phys. Rev.* E **74** 065401